Synthesis of FeWO$_4$ heterogeneous composite by the sol–gel process: enhanced photocatalytic activity on malachite green

Hasna Boudghene Stambouli[1] · Fouad Guenfoud[1] · Amina Benomara[1] · Malika Mokhtari[1] · Mutlu Sönmez-Çelebi[2]

Abstract

Synthesis and characterization of mixed oxide FeWO$_4$ as a photocatalyst in the photodegradation of malachite green (MG) by UV irradiation at 254 nm in a closed reactor was performed. The synthesis was carried out by the sol–gel method (or the citric acid sol–gel method) at room temperature using sodium tungstate(VI) and iron(II) sulfate as precursors. Characterization of the photocatalyst was performed using X-ray diffraction (XRD), FT-IR spectrometry, Scanning electron microscopy coupled with energy dispersive X-ray spectroscopy (SEM-EDXS), BET and X-ray fluorescence (XRF) methods. In order to assess its effectiveness in the degradation of MG, various photo-catalytic tests were carried out. The results obtained showed that the oxide prepared by the sol–gel method has more interesting photocatalytic properties and that the acidity of the medium accelerates the photo-degradation, the optimal conditions were determined such as strongly acidic (pH = 3), and [FeWO$_4$] = 0.5 g L^{-1} with the rate constant k equal to 0.068 min^{-1}.

Keywords FeWO$_4$ catalyst · Sol–gel method · Photocatalysis · Malachite green

Introduction

The protection of our environment inquires a good mastery of the reduction of the pollutants regenerated by the anthropogenic and industrial activities. Owing to their non-polluting nature, advanced oxidation processes constitute a highly effective and clean solution that is included in the green chemistry and the sustainable

✉ Malika Mokhtari
   mokhtarimalika@yahoo.fr

1   Inorganic Chemistry and Environment Laboratory, University of Tlemcen, P.O. Box 119,
    13000 Tlemcen, Algeria

2   Department of Chemistry, Faculty of Science and Arts, University of Ordu, 52200 Ordu, Turkey

development concepts. Catalytic photodegradation or photocatalytic process is a very promising alternative for the elimination of soluble organic compounds, by leading to their total mineralization into carbon dioxide, water and mineral acids, in soft conditions of pressure and temperature [1]. Photocatalytic process using semi-conductor nanoparticles has received considerable attention for the degradation and mineralization of various organic pollutants (dyes, phenols, pesticides and pharmacology products) in aqueous media [2]. Among the several semi-conductors of metallic oxides, TiO_2 [3], ZnO [4], WO_3 [5], Fe_2O_3 [6] and Bi_2O_3 [7] are a widely studied photocatalysts because of their non-toxicity, chemical stability and inertia [8].

Various fields of material science and nano-technology are henceforth strongly oriented towards the importance of the preparation and characterization of nano-inorganic materials and their specific morphology. Currently, many efforts are dedicated to studying metallic tungstate semi-conductors with the general formula MWO_4 (M = Zn, Mn, Cu, Ni, Fe and Cd).This family of materials is potentially applicable in various industrial fields such as humidity sensors [9, 10], catalysis [11, 12], electrochemical electrodes [13] and in the optical domain [14]. Recent studies have established that metallic tungstates serve as photocatalysts for wastewater treatment [15, 16]. The synthesis of MWO_4 can be realised by different techniques, like the hydrothermal synthesis [17], by co-precipitation [18] and by sol–gel method [19]. The main aim of the present work is the synthesis of $FeWO_4$ material by the sol–gel method with a new protocol, and the study of its efficiency in the photocatalytic degradation of the malachite green (MG) which is a model organic dye.

Materials and methods

Materials

Sodium tungstate(VI) dihydrate ($Na_2WO_4 \cdot 2H_2O$) and iron(II) sulfate heptahydrate ($FeSO_4 \cdot 7H_2O$) were used as starting precursors for the preparation of $FeWO_4$ and citric acid powder ($C_6H_8O_7 \cdot H_2O$) was used as the chelating agent in the study. They were obtained from Merck Germany and SD Fine-Chemicals, India and used without further modification.

The dye, malachite green oxalate (MG) with the chemical formula $C_{46}H_{50}N_4 \cdot 3C_2H_2O_4$, MW = 929.02 g mol^{-1}, λ_{max} = 617 nm (extinction coefficient = 1.5×10^5 M^{-1} cm^{-1}), was supplied by Riedel-de Haën. Stock solutions were prepared by dissolving accurately weighed samples of the dye in ultrapure water to give a concentration of 1000 mg L^{-1} and diluting when necessary. It was protected from light and stored at 20 °C.

Synthesis of photocatalyst $FeWO_4$ by the sol–gel method

Tungstate of iron oxide, $FeWO_4$ was synthesized by sol–gel route. 0.02 mol of $Na_2WO_4 \cdot 2H_2O$ and 0.02 mol of $FeSO_4 \cdot 7H_2O$ were dissolved in 20 mL of distilled

water, then 0.04 mol of citric acid powder ($C_6H_8O_7 \cdot H_2O$) was added to the solution. The resulting mixture was then mixed and stirred for 60 min at room temperature. The translucent solution obtained was then placed in an oven at 75 °C until a brownish gel was formed (~ 3 h). The gel was then dried in the oven for 24 h at 100 °C. After preparation of powder, catalyst calcination to remove impurities (i.e. citrate compounds) done at 200 °C for 6 h in the air atmosphere, the sample was stored for use.

Characterization of FeWO$_4$ samples

The synthesized powders were analyzed to determine their crystalline structure, through the X-ray diffraction technique using PAN analytical Empyrean X-ray diffractometer with Cu K$_\alpha$ radiation, $\lambda = 1.250$ Å, and the system operated at 40 kV and 15 mA. The purities of the as-prepared samples were investigated by energy dispersive X-ray spectroscopy (EDXS) analysis and scanning electron microscopy (SEM) using JEOL model JSM-7001F (Tokyo, Japan). Prior to SEM imaging, all samples were dried and coated with gold film in a sputter coater. The BET surface area and Barrett–Joyner–Halenda (BJH) pore volume of the photocatalyst were determined by adsorption–desorption N_2 isotherm measurement at 77 K isotherms using a NOVA1000e at the temperature of the liquid nitrogen. The chemical compositions of the oxide as well as the mass percentage of the elements W and Fe were determined by the FRX technique using Primus from Rigaku. The FTIR spectrum was recorded with a Perkin-Elmer FTIR 1000 spectrometer at room temperature in the frequency range of 400–4000 cm^{-1} with a resolution of 1 cm^{-1}. The photocatalytic activity of the catalyst was monitored using a Perkin Elmer Lambda 25 UV–Vis spectrophotometer.

In addition, UV–Vis diffuse reflectance spectra (DRS) was measured to study the band gap energy of the synthesized catalyst using a diffuse reflectance accessory of UV–Vis spectrophotometer (DRS) (ANALATIKJENA SPECORD 200 PLUS).

Heterogeneous photocatalytic degradation of MG

The photocatalytic tests of FeWO$_4$ were carried out in a glass immersion photochemical reactor charged with 1000 mL of solution/suspension. The reactor was equipped with Pen-Ray Lamps Group Type 1115 (25 W, 18 mA, 254 nm), which was located axially and held in a quartz immersion tube in a MG solution with an initial concentration of 20 mg L^{-1} and a volume of 500 mL. A circulating water jacket was used to cool the irradiation source. Before turning on the illumination, the suspensions were magnetically stirred for 30 min to establish an adsorption–desorption equilibrium between the solid and the solution. At regular times of irradiation, 5 mL of MG solution were taken and centrifuged (5000 rpm) to remove the catalysts. The photodegradation of MG was monitored by measuring the maximum absorption peak at 617 nm using a Lambda 25 UV–Vis spectrometer.

To evaluate the progress of MG mineralization, the chemical oxygen demand (COD) was measured according to the standard methods for examination of water

and wastewater. The chemical oxygen demand (COD) values were determined by open reflux, a dichromate titration method.

Results and discussions

Characterization of the FeWO$_4$

X-ray diffraction

Fig. 1 shows the XRD patterns of the synthesized FeWO$_4$photocatalyst. The strong signature of the diffraction peaks revealed the good crystalline nature of the nano-catalyst. All peaks were indexed to monoclinic FeWO$_4$, with unit cell parameters of a=4.7131 Å, b=5.6990 Å, c=4.9656 Å and α=γ=90°, β>90°, and a space group of P2/c, which is in good agreement with the literature values (JCPDS Card File No. 74-1130). The synthesized photocatalyst is not 100% pure due to the existence of some impurities of Fe$_2$O$_4$.

Morphology and size analysis

SEM images of FeWO$_4$particlesprepared by the sol–gel process and calcined at 200 °C are given in Fig. 2. It can be observed that the morphology of the powder was uniform where the particle size is approximately 20–30 nm. According to the images obtained the material is characterized by homogenous distribution with crystalline structure. The chemical compositions of O, W and Fe in the synthesized sample were again confirmed by EDXS (Fig. 2, Table 1).
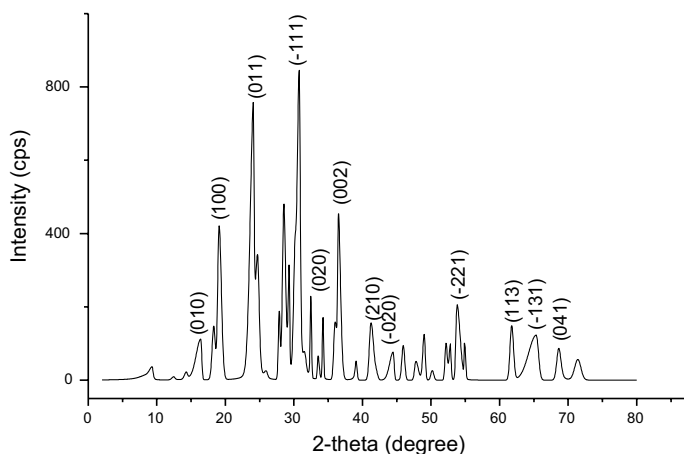

Fig. 1 XRD pattern of prepared FeWO$_4$ powders calcined at 200 °C for 6 h in the air atmosphere
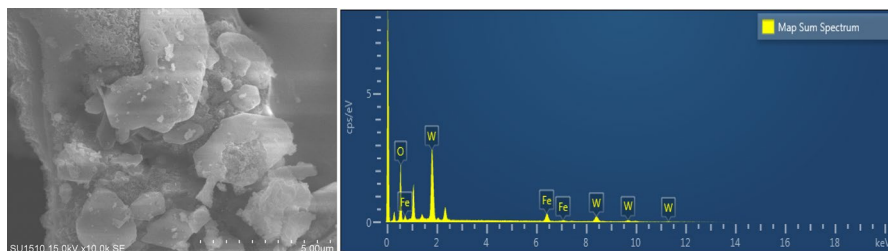
Fig. 2 SEM images and EDXS chemical analysis of FeWO$_4$

Table 1 The chemical composition of O, W and Fe in the synthesized sample were again confirmed by EDXS

Element	Line type	Weight %	Weight % sigma	Atomic %
O	K series	33.28	041	79.34
Fe	K series	14.35	0.39	9.80
W	M series	52.37	0.45	10.86
Total		100.00		100.00

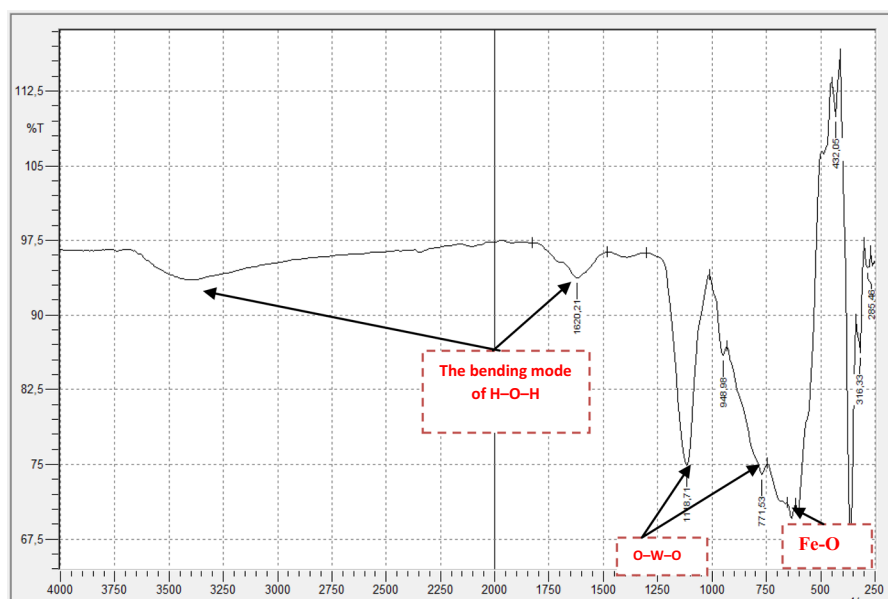**Fig. 3** FTIR spectra of the photocatalyst FeWO$_4$

FTIR spectroscopy

FTIR spectra in the range of 4000–400 cm^{-1} were recorded for FeWO$_4$ and is shown in Fig. 3. The bands positioned at 771 and 948 cm^{-1} were associated to the
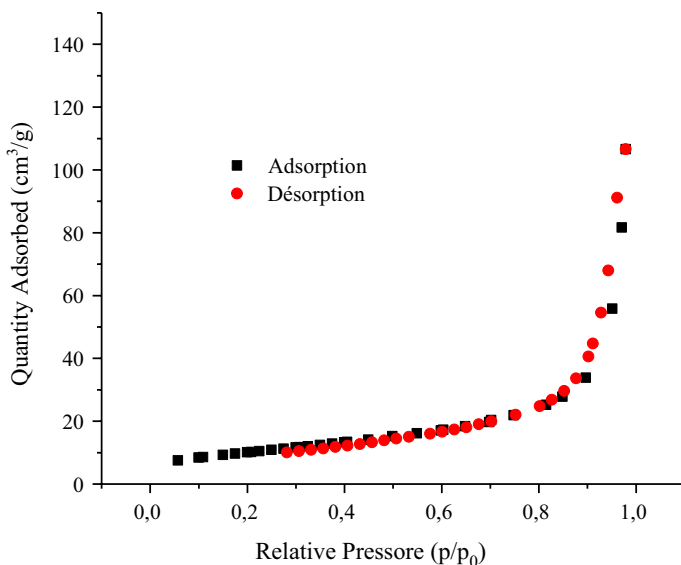
Fig. 4 Nitrogen adsorption/desorption isotherm of FeWO$_4$calcined at 200 °C

Table 2 Specific surface area (S), pore volume (V), and average pore diameter (D) of FeWO$_4$	Photocatalyst	FeWO$_4$
	S (m^2 g^{-1})	36.5848
	V (cm^3 g^{-1})	0.142173
	D (nm)	150.635

O–W–O vibration mode and the W–O bond stretching, respectively [20]. The band at 567 cm^{-1} is related to the Fe–O bending vibration [21]. The bands at around 3423 cm^{-1} and 1620 cm^{-1} can be assigned to the H–O–H stretching modes and bending vibration of the free or adsorbed water, respectively [17].

BET surface area analysis

The N$_2$ adsorption–desorption isotherms of FeWO$_4$ prepared by sol–gel method are illustrated in Fig. 4, which are categorized as type IV isotherms based on the Brunauer–Deming–Deming–Teller (BDDT) categorization[22]. These results implied that mesopores and macropores were formed in the as-prepared materials. Table 2 shows the specific surface area (S) measured by the BET method, the pore volume (V), and the average pore diameter (D). The larger pore volume and BET specific surface area confirmed that the photocatalyst structure possessed an increased number of active sites [23]. Despite the low specific surface of our material, the mesoporous nature of FeWO$_4$ allowed the rapid diffusion of the reactant and

the product of the photocatalytic reaction, which consequently improves the reaction rate.

X-ray fluorescence analysis

X-ray fluorescence analysis was used to determine the concentration of Fe and W atoms in the $FeWO_4$ oxide. The results of the X-ray fluorescence analysis showed that the weight content of Fe and W is 18.97% and 64.33% respectively. Based on these data, it can be concluded that the synthesis of $FeWO_4$ composite is relatively successful with the desired composition or percentage.

Point of zero charge

The interpretation of the pH effects on the efficiency of the photodegradation process of dyes is a very difficult task because of its multiple roles [24]. The changing of the pH of the environment modifies the surface charge of the catalyst, the reagent speciation and the equilibrium of the radical reactions [25].The surface charge is an important parameter when it comes to studying surface processes such as photocatalysis. For all types of catalysts, always exists a value called the zero charge point where the surface charge is zero.

Consequently, at $pH < pH_{PZC}$ the surface is charged positively, it will exercise an electrostatic attraction on the present anions in the solution, and vice versa if the $pH > pH_{PZC}$ [26]. The pH of the solution influences the surface load of the catalyst [26] and the size of the particles that aggregate in water [27]. When the $pH = pH_{PZC}$, the charge on the surface of the catalyst disappears. There is therefore much less electrostatic interaction between the particles, which favors the phenomenon of aggregation [27]. It was observed that the pH has a certain influence upon the valence band through shifting it by 0.059 eV per point of pH [28, 29].

The zero charge point can experimentally be determined by different processes according to the used electrolyte. In our study, we determined it by the titration process. For this purpose, 50 mL of a NaCl solution (0.01 mol L^{-1}) was added into several Erlenmeyer. The initial pH of the solutions was varied between 4 and 12 by the addition of a solution of NaOH or HCl (0.1 mol L^{-1}), after that 50 mg of the material were added to each bottle, the suspensions being maintained under stirring, at room temperature for 24 h, and the final pH was than determined [30].

Fig. 5 represents the obtained results of ΔpH ($pH_{final} - pH_{initial}$) in terms of the $pH_{initial}$ of the synthesised material. The value of the pH_{PZC} of $FeWO_4$ is equal to 4. When the pH of the solution is different than the pH_{PZC}, the surface is charged and this will have an important effect on the degradation rate, it is positively charged at a pH under the pH_{PZC} and vice versa at a pH above the pH_{PZC} where the surface is anionic.

Optical properties

The optical properties of $FeWO_4$ were measured by DRS The diffused reflectance spectrum is recorded in the range (300–1100 nm) the spectrum shows that the
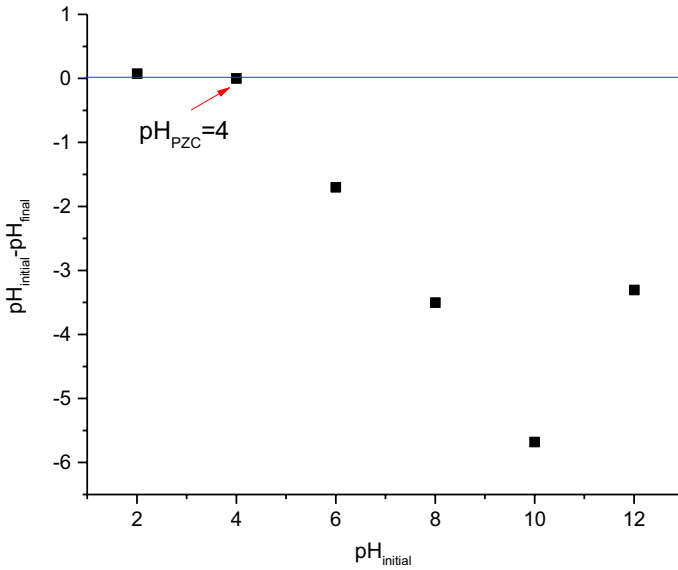
Fig. 5 Plot for the determination of pH_{pzc} of $FeWO_4$

material has a maximum reflectance (99.06%) in the visible field at $\lambda = 295$ nm. The band gap energy (E_g) can be estimated by the equation of $\alpha h\upsilon = A(h\upsilon - E_g)^n$.

Here A is a constant, $n = 2$ for the direct transition, $h\upsilon$ is the incident photon energy, and α is the absorption coefficient [14, 15]. Fig. 6 gives the plot of $(\alpha h\upsilon)^2$
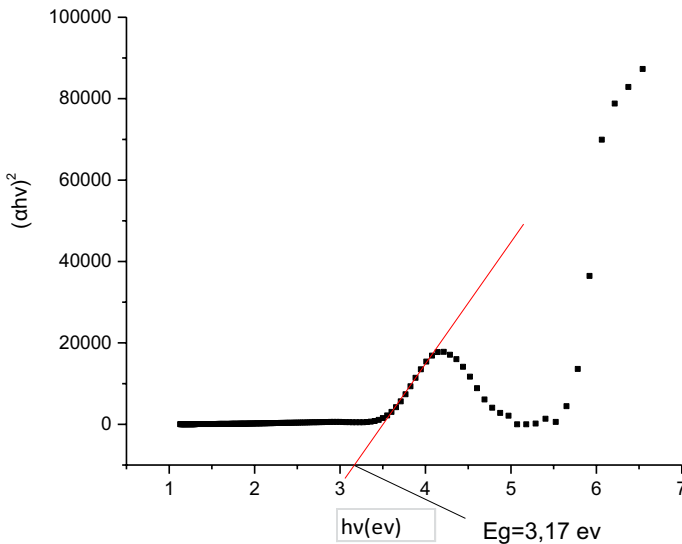

Fig. 6 Band gap energy determination of $FeWO_4$

versus hʋ. The intercept of the tangent to the plot illustrates an approximation value of E_g for $FeWO_4$. E_g is about 3.17 eV.

Study of the photocatalytic activity of $FeWO_4$

Effect of initial pH

The pH parameter is a very important operational variable for the treatment of waste water. It determines the superficial properties of the solids and the state of the pollutant to be degraded according to its pKa [31]. The pH effect on the photocatalytic degradation of the MG by the synthesized material has been realised at different pH values (acid, natural pH and neutral pH).

The pH influence on the MG degradation kinetics by photocatalysis was studied in a range between 3 and 7. The pH was adjusted by the addition of NaOH (1 mol L^{-1}) for the neutral medium and H_2SO_4 (1 mol L^{-1}) for the acid medium. As shown in Fig. 7, it can clearly state that the MG photoctalytic degradation rate was significantly enhanced at pH=3 with a yield of 97.48%, and it decreased when the pH rises.

At pH=3, the MG dye is neutral ($pK_a = 1.3$) and the photocatalyst surface is positive ($pH_{pzc} = 4$). Thus, this led to an electrostatic repulsion between the dye and the catalyst's surface leading to an adsorption lowering at the surface of $FeWO_4$.

Generally, pH=3 is the optimal pH for all the photo-Fenton homogeneous reactions, but most of the researchers find that the pH=3 is also optimal for the
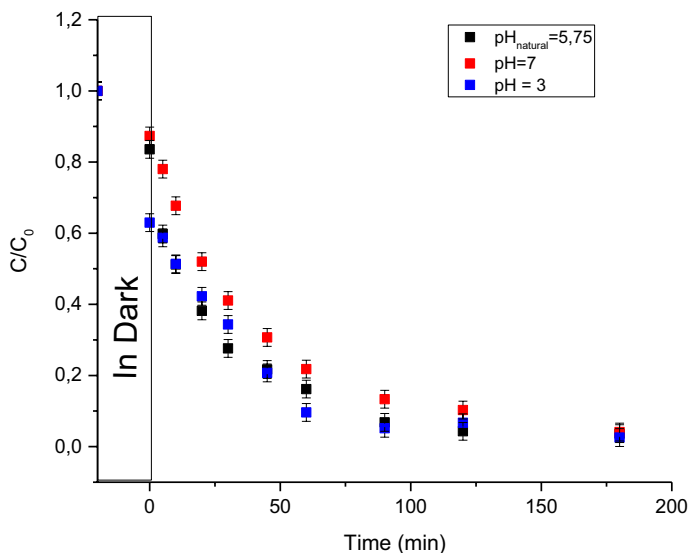

Fig. 7 Effect of pH on photocatalytic degradation of MG under the condition: [MG]=20 mg L^{-1}, $V_{solution}$=500 mL, [catalyst]=0.25 g L^{-1} and 25 W $UV_{254\ nm}$ irradiation

heterogeneous systems with catalysts containing Fe in their structures, as the Fenton heterogeneous catalysts [32].

The enhanced oxidation efficiency at pH = 3 can be attributed to the higher oxidation potential of the hydroxyl radicals, the most dissolved fraction of iron species, the H_2O_2 stability in acidic solution that cannot be immediately decomposed into H_2O and O_2, and the formation of an interne sphere of metallic oxides-pollutant complexes that favour the reaction [33].

Effect of catalyst concentration

The photocatalytic degradation rate is directly related to the catalyst quantity in the weak concentrations field. However, after a certain value, the reaction rate becomes independent from the catalyst mass [34, 35]. Therefore, the influence of the concentration of $FeWO_4$ on the photodegradation of the MG was studied between 0.125 and 2 g L^{-1}. The obtained results in the operating conditions presented in Fig. 8 show that the degradation rate is at its maximum (98.41%) at an concentration (0.5 g L^{-1}) of $FeWO_4$. Beyond this concentration, the amount of degradation decreases slightly due to the bad penetration of the UV rays and the screen effect phenomenon becomes predominant [36]. Huang added that the increase of the concentration of the catalyst beyond the optimum value can drive to the agglomeration of the catalyst particles, thus the surface of the catalyst becomes unavailable for the adsorption of photons and the degradation rate decreases [37].
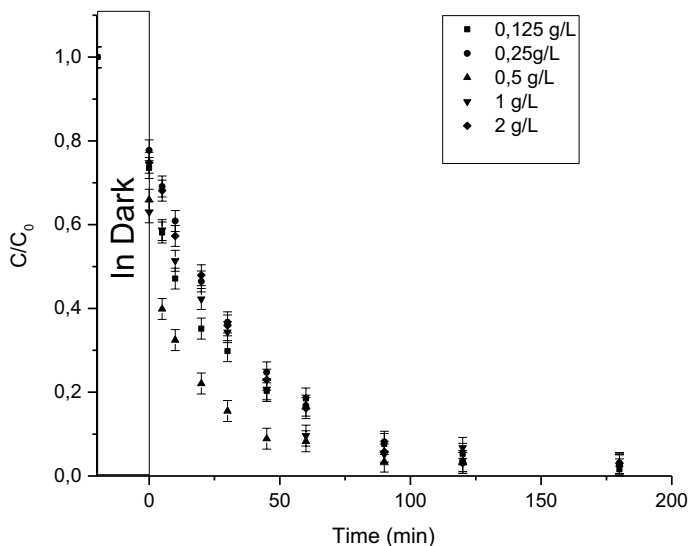

Fig. 8 Effect of $FeWO_4$ concentration on the degradation of MG under the condition: [MG] = 20 mg L^{-1}, $V_{solution}$ = 500 mL, pH = 3 and 25 W $UV_{254\,nm}$ irradiation

Kinetics and the monitoring of photodegradation by UV–Vis spectrophotometer

The degradation kinetics of dye would be established using the following formula (Eq. 1) [38]:

$$Y_t = X\,e^{-kt} + E \tag{1}$$

With X is termed the amplitude, k is the first order rate constant, and E is the endpoint the results are shown in Fig. 9.

In addition, the integration in time (in interval τ) is a key question when the response time of the monitoring method is not much faster than the process studied. The integrated observation is described by Eq. 2 [38]:

$$_t^\tau Y = \frac{1}{\tau} \int_t^{1+\tau} \left(X e^{-ks} + E \right) ds = \frac{1 - e^{-k\tau}}{k\tau} X e^{-kt} + E \tag{2}$$

Here (X) is the calculated amplitude; (E) is the endpoint; (k) is the kinetic constants and R^2 value (coefficient of determination) are shown in Table 3.

The best kinetic rate was obtained with 0.5 g L^{-1} of the catalyst with a kinetic constant k = 0.068 min^{-1}.
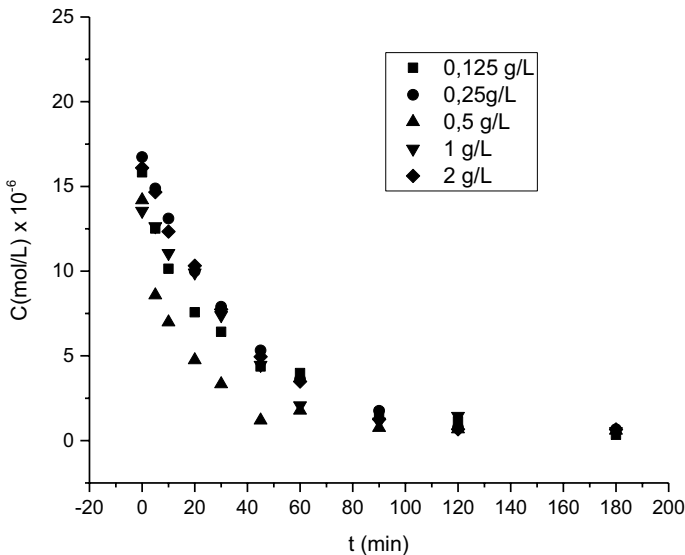

Fig. 9 Kinetic degradation of MG, [MG] = 20 mg L^{-1}, $V_{solution}$ = 500 mL, pH = 3 and 25 W $UV_{254\ nm}$ irradiation

Table 3 Kinetic results of the dye degradation

$[FeWO_4]$ (g L^{-1})	E	Standard errors	X	Standard errors	k (min^{-1})	Standard errors	R^2	Standard errors
0.125	9.29×10^{-7}	4.74×10^{-7}	1.39×10^{-5}	6.29×10^{-7}	0.0327	3.93×10^{-3}	0.984	3.77×10^{-12}
0.25	2.86×10^{-7}	1.11×10^{-7}	1.65×10^{-5}	1.31×10^{-7}	0.0264	5.74×10^{-4}	0.999	1.54×10^{-13}
0.5	9.59×10^{-7}	3.44×10^{-7}	1.24×10^{-5}	6.72×10^{-7}	0.0680	8.96×10^{-3}	0.978	3.93×10^{-12}
1	7.23×10^{-8}	6.45×10^{-7}	1.40×10^{-5}	7.26×10^{-7}	0.0240	3.47×10^{-3}	0.980	4.51×10^{-12}
2	6.68×10^{-8}	2.87×10^{-7}	1.62×10^{-5}	3.33×10^{-7}	0.0258	1.14×10^{-3}	0.996	9.82×10^{-13}

Recycling of photocatalyst, COD and UV–Vis spectra

The photocatalyst stability during the photodegradation process is a key factor for a convenient application. In order to evaluate the stability of $FeWO_4$, recycling photocatalytic activity tests have been realised and repeated three times, using the recuperated photocatalyst in the same optimal conditions.

The obtained results are represented in Fig. 10a. This figure shows that there is no notable decreasing in the photocatalyst efficiency until the third cycle. It indicates that the synthesised $FeWO_4$ is a stable and reusable photocatalyst [39]. The slight diminution in the MG degradation could be also due to the occupation of the active sites by the intermediate adsorption, and the waste part of the photocatalyst during the recycling test process [40].

Fig. 10b show the absorption spectra of MG (pH = 3) at different time intervals under optimal conditions. It is seen that absorbance at $\lambda_{max} = 620$ nm progressively
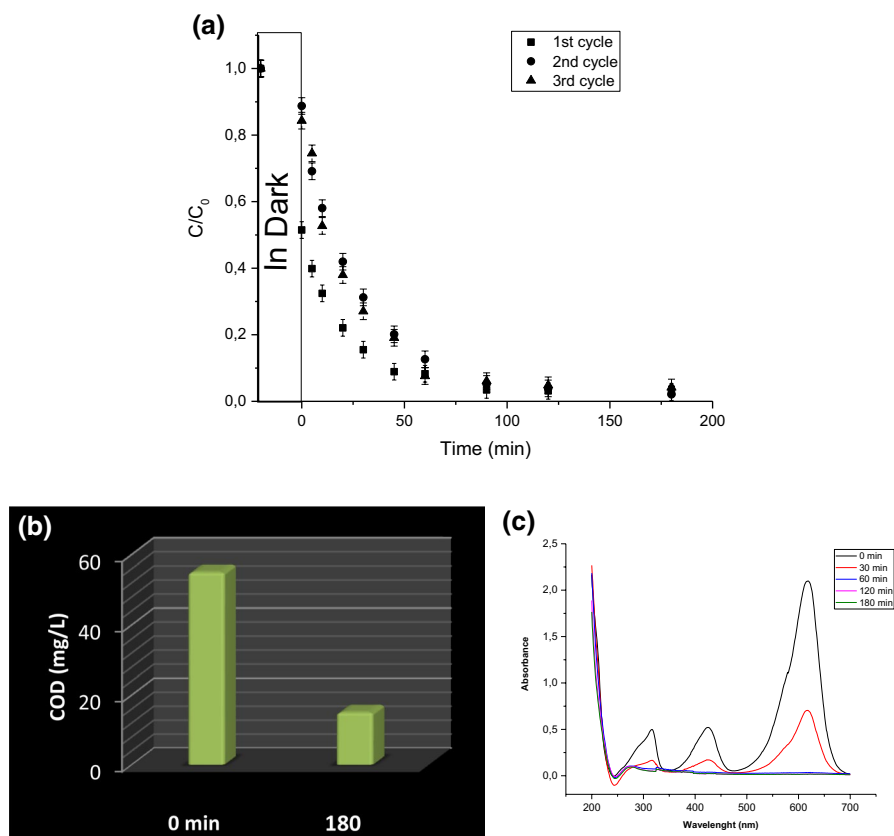

Fig. 10 **a** Cyclic runs showing photocatalytic degradation of MG by $FeWO_4$. **b** COD degradation of malachite green. **c** UV–Visible spectra of malachite green (MG) during degradation photocatalytic at different time intervals under optimal conditions: [MG] = 20 mg L^{-1}, $V_{solution}$ = 500 mL, pH = 3, [catalyst] = 0.5 g L^{-1} and 25 W $UV_{254\,nm}$ irradiation. (Color figure online)

decreases as the irradiation time increases. This indicates that the pollutant is successfully degrading on the surface of photocatalyst with time. We can see the disappearance of all the characteristic bands of the dye which means the degradation of the dye.

The experimental results showed that the chemical oxygen demand decreased from 55 mg L^{-1} at 0 min to 21 mg L^{-1} after 180 min of treatment with a degradation of 73% (Fig. 10c).

Conclusion

The main aim of this work is to study the photocatalytic degradation of a waste water sample polluted by malachite green (MG) dye in heterogeneous phase using the $FeWO_4$ as the catalyst. The material was synthesized by the sol–gel route and calcined at 200 °C. This method provides a simple route for material synthesis. According to the XRD, SEM–EDX and FTIR results, a better crystallinity of the material was obtained with a regular structure.

The several executed photocatalytic tests gave very interesting results, the photocatalytic degradation was higher in acidic medium (pH = 3.00) with a degradation yield of 97.47% after 3 h. Furthermore, the cycle experience shows that $FeWO_4$ is stable after three cycles. Finally, in our study, we showed that the degradation reaction of the malachite green follows a pseudo first order kinetic.

References

1. Lad VN, Murthy ZVP (2020) 1—Advanced materials for photocatalytic applications: the challenge ahead. In: Mustansar Hussain C, Mishra AK (eds) Handbook of smart photocatalytic materials. Elsevier, Amsterdam, pp 3–8. https://doi.org/10.1016/B978-0-12-819051-7.00001-4
2. Collazzo GC, Foletto EL, Jahn SL, Villetti MA (2012) Degradation of Direct Black 38 dye under visible light and sunlight irradiation by N-doped anatase TIO_2 as photocatalyst. J Environ Manag 98:107–111. https://doi.org/10.1016/j.jenvman.2011.12.029
3. Lee S-Y, Park S-J (2013) TiO_2 photocatalyst for water treatment applications. J Ind Eng Chem 19(6):1761–1769. https://doi.org/10.1016/j.jiec.2013.07.012
4. Karunakaran C, Rajeswari V, Gomathisankar P (2011) Optical, electrical, photocatalytic, and bactericidal properties of microwave synthesized nanocrystalline Ag–ZnO and ZnO. Solid State Sci 13(5):923–928. https://doi.org/10.1016/j.solidstatesciences.2011.02.016
5. Qamar M, Yamani ZH, Gondal MA, Alhooshani K (2011) Synthesis and comparative photocatalytic activity of Pt/WO_3 and Au/WO_3 nanocomposites under sunlight-type excitation. Solid State Sci 13(9):1748–1754. https://doi.org/10.1016/j.solidstatesciences.2011.07.002
6. Qurashi A, Zhong Z, Alam MW (2010) Synthesis and photocatalytic properties of α-Fe_2O_3 nanoellipsoids. Solid State Sci 12(8):1516–1519. https://doi.org/10.1016/j.solidstatesciences.2010.05.001
7. Li E-J, Xia K, Yin S-F, Dai W-L, Luo S-L, Au C-T (2011) Preparation, characterization and photocatalytic activity of Bi_2O_3–MgO composites. Mater Chem Phys 125(1):236–241. https://doi.org/10.1016/j.matchemphys.2010.09.013

8. Vignesh K, Hariharan R, Rajarajan M, Suganthi A (2013) Photocatalytic performance of Ag doped SnO$_2$ nanoparticles modified with curcumin. Solid State Sci 21:91–99. https://doi.org/10.1016/j.solidstatesciences.2013.04.017

9. Li Y, Li X, Tang Z, Wang J, Yu J, Tang Z (2016) Potentiometric hydrogen sensors based on yttria-stabilized zirconia electrolyte (YSZ) and CdWO$_4$ interface. Sens Actuators B 223:365–371. https://doi.org/10.1016/j.snb.2015.09.110

10. Ganiger SK, Chaluvaraju BV, Ananda SR, Murugendrappa MV (2018) A feasibility study of polypyrrole/zinc tungstate (ceramics) nano composites for D.C. conductivity and as a humidity sensor. Mater Today 5(13):2803–2810. https://doi.org/10.1016/j.matpr.2018.01.068

11. Paul A, Devi M, Dhar SS (2020) Incorporation of nanosized ZnWO$_4$ and Fe$_3$O$_4$ on graphitic carbon nitride to fabricate a novel, highly active magnetically recoverable catalyst in Claisen–Schmidt condensation. J Phys Chem Solids 136:109117. https://doi.org/10.1016/j.jpcs.2019.109117

12. Fatima B, Siddiqui SI, Ahmed R, Chaudhry SA (2019) Green synthesis of f-CdWO$_4$ for photocatalytic degradation and adsorptive removal of Bismarck Brown R dye from water. Water Resour Ind 22:100119. https://doi.org/10.1016/j.wri.2019.100119

13. Harichandran G, Divya P, Yesuraj J, Muthuraaman B (2020) Sonochemical synthesis of chain-like ZnWO$_4$ nanoarchitectures for high performance supercapacitor electrode application. Mater Charact 167:110490. https://doi.org/10.1016/j.matchar.2020.110490

14. Lalić MV, Popović ZS, Vukajlović FR (2011) Ab initio study of electronic, magnetic and optical properties of CuWO$_4$ tungstate. Comput Mater Sci 50(3):1179–1186. https://doi.org/10.1016/j.commatsci.2010.11.018

15. Raizada P, Sharma S, Kumar A, Singh P, Parwaz Khan AA, Asiri AM (2020) Performance improvement strategies of CuWO$_4$ photocatalyst for hydrogen generation and pollutant degradation. J Environ Chem Eng 8(5):104230. https://doi.org/10.1016/j.jece.2020.104230

16. Shad NA, Sajid MM, Amin N, Javed Y, Akhtar K, Ahmad G, Hassan S, Ikram M (2019) Photocatalytic degradation performance of cadmium tungstate (CdWO$_4$) nanosheets-assembly and their hydrogen storage features. Ceram Int 45(15):19015–19021. https://doi.org/10.1016/j.ceramint.2019.06.142

17. Kovács TN, Pokol G, Gáber F, Nagy D, Igricz T, Lukács IE, Fogarassy Z, Balázsi K, Szilágyi IM (2017) Preparation of iron tungstate (FeWO$_4$) nanosheets by hydrothermal method. Mater Res Bull 95:563–569. https://doi.org/10.1016/j.materresbull.2017.08.031

18. Quintana-Melgoza JM, Cruz-Reyes J, Avalos-Borja M (2001) Synthesis and characterization of NiWO$_4$ crystals. Mater Lett 47(4):314–318. https://doi.org/10.1016/S0167-577X(00)00272-X

19. Shang H, Bliss M, Heald S, Sham T, Heigl F, Cao G (2007) Dense and optical transparent CdWO$_4$ films by sol-gel processing for scintillation applications. J Mater Res 22(6):1527–1536

20. Juliet Josephine Joy J, Victor Jaya N (2013) Structural, magnetic and optical behavior of pristine and Yb doped CoWO$_4$ nanostructure. J Mater Sci 24(6):1788–1795. https://doi.org/10.1007/s10854-012-1013-1

21. Li S-K, Hou X-C, Huang F-Z, Li C-H, Kang W-J, Xie A-J, Shen Y-H (2013) Simple and efficient synthesis of copper(II)-modified uniform magnetic Fe$_3$O$_4$@SiO$_2$ core/shell microspheres for immobilization of cellulase. J Nanopart Res 15(11):2013. https://doi.org/10.1007/s11051-013-2013-7

22. Brunauer S, Deming LS, Deming WE, Teller E (1940) On a theory of the van der Waals adsorption of gases. J Am Chem Soc 62(7):1723–1732. https://doi.org/10.1021/ja01864a025

23. Yu C, Wen M, Tong Z, Li S, Yin Y, Liu X, Li Y, Liang T, Wu Z, Dionysiou DD (2020) Synthesis and enhanced photocatalytic performance of 0D/2D CuO/tourmaline composite photocatalysts. Beilstein J Nanotechnol 11:407–416. https://doi.org/10.3762/bjnano.11.31

24. Konstantinou IK, Albanis TA (2004) TiO$_2$-assisted photocatalytic degradation of azo dyes in aqueous solution: kinetic and mechanistic investigations: a review. Appl Catal B 49(1):1–14. https://doi.org/10.1016/j.apcatb.2003.11.010

25. Zhan H, Chen K, Tian H (1998) Photocatalytic degradation of acid azo dyes in aqueous TiO$_2$ suspension II. The effect of pH values. Dyes Pigment 37(3):241–247. https://doi.org/10.1016/S0143-7208(97)00063-6

26. Fernández A, Lassaletta G, Jiménez VM, Justo A, González-Elipe AR, Herrmann JM, Tahiri H, Ait-Ichou Y (1995) Preparation and characterization of TiO$_2$ photocatalysts supported on various rigid supports (glass, quartz and stainless steel). Comparative studies of photocatalytic activity in water purification. Appl Catal B 7(1):49–63. https://doi.org/10.1016/0926-3373(95)00026-7

27. Malato S, Fernández-Ibáñez P, Maldonado MI, Blanco J, Gernjak W (2009) Decontamination and disinfection of water by solar photocatalysis: recent overview and trends. Catal Today 147(1):1–59

28. Muneer M, Theurich J, Bahnemann D (1999) Formation of toxic intermediates upon the photocatalytic degradation of the pesticide diuron. Res Chem Intermed 25(7):667–683

29. Malato S, Blanco J, Richter C, Curcó D, Gimenez J (1997) Low-concentrating CPC collectors for photocatalytic water detoxification: comparison with a medium concentrating solar collector. Water Sci Technol 35(4):157–164. https://doi.org/10.1016/S0273-1223(97)00021-8

30. Guenfoud F, Ramdane AC, Belmir C, Sönmez-Çelebi M (2021) TiCe$_{0.667}$O$_3$ particles: sol–gel synthesis, characterization, and kinetics of photocatalytic decomposition of diazo dye—Reactive Black 5 (RB5). Desalin Water Treat 208:399–406

31. Chu W, Choy WK, So TY (2007) The effect of solution pH and peroxide in the TiO$_2$-induced photocatalysis of chlorinated aniline. J Hazard Mater 141(1):86–91. https://doi.org/10.1016/j.jhazmat.2006.06.093

32. Gonzalez-Olmos R, Martin MJ, Georgi A, Kopinke F-D, Oller I, Malato S (2012) Fe-zeolites as heterogeneous catalysts in solar Fenton-like reactions at neutral pH. Appl Catal B 125:51–58. https://doi.org/10.1016/j.apcatb.2012.05.022

33. Jung YS, Lim WT, Park JY, Kim YH (2009) Effect of pH on Fenton and Fenton-like oxidation. Environ Technol 30(2):183–190. https://doi.org/10.1080/09593330802468848

34. Dionysiou DD, Suidan MT, Bekou E, Baudin I, Laîné J-M (2000) Effect of ionic strength and hydrogen peroxide on the photocatalytic degradation of 4-chlorobenzoic acid in water. Appl Catal B 26(3):153–171. https://doi.org/10.1016/S0926-3373(00)00124-7

35. Parra S, Olivero J, Pulgarin C (2002) Relationships between physicochemical properties and photoreactivity of four biorecalcitrant phenylurea herbicides in aqueous TiO$_2$ suspension. Appl Catal B 36(1):75–85. https://doi.org/10.1016/S0926-3373(01)00283-1

36. Hasnat MA, Uddin MM, Samed AJF, Alam SS, Hossain S (2007) Adsorption and photocatalytic decolorization of a synthetic dye erythrosine on anatase TiO$_2$ and ZnO surfaces. J Hazard Mater 147(1):471–477. https://doi.org/10.1016/j.jhazmat.2007.01.040

37. Huang M, Xu C, Wu Z, Huang Y, Lin J, Wu J (2008) Photocatalytic discolorization of methyl orange solution by Pt modified TiO$_2$ loaded on natural zeolite. Dyes Pigment 77(2):327–334. https://doi.org/10.1016/j.dyepig.2007.01.026

38. Lente G (2015) Deterministic kinetics in chemistry and systems biology: the dynamics of complex reaction networks. Springer briefs in molecular science. Springer, Cham

39. Lavand AB, Bhatu MN, Malghe YS (2019) Visible light photocatalytic degradation of malachite green using modified titania. J Market Res 8(1):299–308. https://doi.org/10.1016/j.jmrt.2017.05.019

40. Benomara A, Guenfoud F, Mokhtari M (2019) Removal of methyl violet 2B by FePO$_4$ as photocatalyst. React Kinet Mech Catal 127(2):1087–1099. https://doi.org/10.1007/s11144-019-01607-8

Publisher's Note Springer Nature remains neutral with regard to jurisdictional claims in published maps and institutional affiliations.